Document downloaded from:

http://hdl.handle.net/10251/60018

This paper must be cited as:

Payri González, F.; Olmeda, P.; Arnau Martínez, FJ.; Dombrovsky, A.; Smith, L. (2014). External heat losses in small turbochargers: Model and experiments. Energy. 71:534-546. doi:10.1016/j.energy.2014.04.096.

The final publication is available at

http://dx.doi.org/10.1016/j.energy.2014.04.096

Copyright Elsevier

Additional Information

External heat losses in small turbochargers: model and experiments

Francisco Payri, Pablo Olmeda*, Francisco J. Arnau, Artem Dombrovsky

CMT-Motores Térmicos, Universitat Politècnica de València, Camino de Vera s/n. 46022 València, Spain

Les Smith

Jaguar Land Rover Ltd, Abbey Road, Whitley, Coventry, CV3 4LF, UK

Abstract

The behavior of small turbochargers is deeply affected by heat transfer phenomena. The external heat losses of these engines are studied and a simplified model that takes into account both radiation and convective mechanisms has been proposed. The model has been adjusted in a turbocharger test bench for two different turbochargers, later on it has been validated against experimental measurements on an engine test bench. Finally, the model has been used to estimate the most important external heat flows among the different elements of the turbocharger.

Keywords: Turbocharger, External heat transfer, Radiation, experimental analysis

Nomenclature

A	Area	m^2
c	specific heat capacity	$\mathrm{J \cdot kg^{-1} \cdot K^{-1}}$
h	convective coefficient	$\mathrm{W \cdot m^{-2} \cdot K^{-1}}$
h	Specific enthalpy	$\mathrm{J \cdot kg^{-1}}$

*Corresponding author. Tel: +34963877650; fax: +34963877659
Email address: pabolgon@mot.upv.es (Pablo Olmeda)
URL: www.cmt.upv.es (Pablo Olmeda)

K	Conductance	$\mathrm{W \cdot K^{-1}}$
L	Length	m
$\dot{m}$	Mass flow	$\mathrm{kg \cdot s^{-1}}$
r	Radius	m
T	Temperature	K
$\dot{Q}$	Heat flow	W

Dimensionless numbers

F	View factor
Gr	Grasshof number
Nu	Nusselt number
Pr	Prandtl number
Ra	Rayleigh number
Re	Reynolds number

Greeks symbols

α	Percentage	$-$
ϵ	Emissivity	$-$
ν	Kinematic viscosity	$\mathrm{m^2 \cdot s^{-1}}$
ϕ	Diameter	m
σ	Steffan-Boltzman constant	$\mathrm{W \cdot m^{-2} \cdot K^{-4}}$

Subscripts

air	Air
amb	Refers to ambient
C	Refers to compressor
CN	Natural / Free convection
CF	Forced convection
ext	Refers to external surface
gas	Gas
H	Refers to housing
$H1$	Refers to housing node close to turbine
$H2$	Refers to central housing node

$H3$	Refers to housing node close to compressor
i, j, k, n	Generic element
IC	Compressor inlet
IO	Oil inlet
IT	Turbine inlet
lat	Refers to lateral surface
oil	Oil
OC	Compressor outlet
OO	Oil outlet
OT	Turbine outlet
r	Refers to radiation
s	Shield
T	Refers to turbine
unb	Unbalance
w	Refers to wall temperature
$1, 2$	Element number

1. Introduction

Nowadays, internal combustion engines (ICE) face with two main challenges: the reduction of fuel consumption and pollutant emissions. With this purpose different techniques have appeared to better optimize the combustion process: high pressure fuel injection systems [1], multiple injections [2], high boost pressure [3], two stage turbocharging [4],EGR [5], variable valve timing [6], high swirl ratios [7], new clean fuels [8], etc. In this framework, the optimization of engine external systems can play an important role. One of the most used among these systems is turbocharging. In order to predict accurately engine behavior is necessary to predict the behavior of turbocharger [9]. This behavior must bear in mind at least two main factors: mechanical power transferred from the turbine to the compressor through the central axis [10] and the heat flows between these two elements due to the differences in the working fluids temperatures. This work falls in the second item trying to contribute to the knowledge of the external heat losses (convection and radiation) in small turbochargers.

Bohn [11] performed a parametric study for a passenger car turbocharger in order to analyze qualitatively the heat flux between turbine and compressor, finding that, in their measurements, and due to turbocharger geometry, radiation had a small influence on the total heat flux.

On the contrary, Baines [12] assured that the heat transfers of greatest magnitude and significance to turbocharger performance on-engine are external from the turbine to the environment, and internal from the turbine to the bearing housing and that radiation makes an appreciable contribution to the external heat transfer. They assumed that external heat transfer could be calculated as the energy unbalance in their measurements, but no model of radiation to ambient was presented.

In [13], authors suggest that the radiation and natural convection from the engine to the turbocharger are relevant but they do not quantify it, since they would need further investigation. In other work [14], the heat fluxes through the turbocharger were evaluated by means of well known correlations available in literature, but some of them were not described in the paper.

On other research works [15], authors simulated heat flows from the turbine and to the compressor artificially and assuming only external heat transfer from turbine to ambient.

In this work a simplified external heat transfer model taking into account all the possible heat fluxes in a turbocharger is developed. The first part of the work concerns about the experimental methodology and the main parameters measured in order to characterize external heat transfer flow. Then, the proposed external heat transfer model of the turbocharger is presented. After that, results are presented. Later, an analysis of the different heat fluxes is performed by using the model and, finally, the main conclusions of the work are outlined.

2. Experimental tools

The experimental tools used in this work consist on two different test rigs (a turbocharger test rig, which is briefly described in section 2.1, and an engine test rig, described in section 2.2) and two different turbochargers units, whose main characteristics are mentioned on section 2.3.

2.1. Turbocharger test rig

The measurement on turbocharger test rig has been used in order to adjust the proposed model. Figure 1 shows the layout of a continuous air flow test bench [10]. It is composed by the following parts:

- A screw compressor with a maximum mass flow capacity of 0.2 $kg \cdot s^{-1}$, at a maximum discharging pressure of 3.5 bar (gauge), which provides the mass flow to the turbine. The mass flow rate is controlled by the screw compressor speed or an electronic discharge valve (placed after the screw compressor). The valve is used when a mass flow lower than the minimum supplied by the screw compressor is required. The extra flow is directly discharged to the atmosphere.

- The mass flow is heated in parallel by five tube-type electrical heaters. The flow through each of the heaters is regulated and balanced by means of valves placed on the heater's inlet ports. This system can reach up to 720 K at the maximum mass flow rate. This hot flow is collected in a plenum and conducted to the turbine inlet.

- After passing through the turbine, the air is cooled by means of a heat exchanger in order to allow the mass flow measurement by high accuracy hot film flow meters. All flow meters in the installation have been previously calibrated.

- The turbocompressor sucks air from the atmosphere. The air passes first through a filter and then its flow rate is measured. Downstream of the compressor, there is an electronically driven backpressure valve. Hereinafter compressor refers only to turbocompressor.

- An independent lubrication system is used to control oil flow rate, pressure (by means of an oil pump and a pressure control valve) and temperature (by using an electrical heater and a cooler). The oil mass flow rate is measured by means of a Coriolis flow meter. Lubrication inlet and outlet temperatures are measured by means of low uncertainty platinum resistance temperature sensors. The independent lubrication system is conditioned to take periodic samples of oil in order to characterize its properties (viscosity, density and specific heat capacity variations with temperature).

- Temperature and pressure sensors are installed on the inlet and the outlet pipes of the compressor and the turbine according to SAE J1723 [16] and SAE J1826 [17] standards.

- An independent cooling system (when turbocharger is water cooled) is used to control coolant flow rate, pressure (by means of a coolant pump and a pressure control valve) and temperature (by using an electrical heater and a cooler). Coolant inlet and outlet temperatures are measured by means of low uncertainty platinum resistance temperature sensors.

- Wall temperatures in three different radial planes and in five different axial planes are acquired by means of K-type thermocouples.

Table 1 shows representative information about the measurement range and uncertainty of the main sensors used in the test bench.

The tests performed on this rig have been divided into two main groups, namely:

1. Almost-adiabatic tests [18]. The main objective in this kind of tests is to decouple mechanical losses and heat transfer in the turbocharger under study [19]. In this way, heat transfer is minimized and the oil enthalpy drop corresponds mainly to mechanical losses in the turbocharger. This

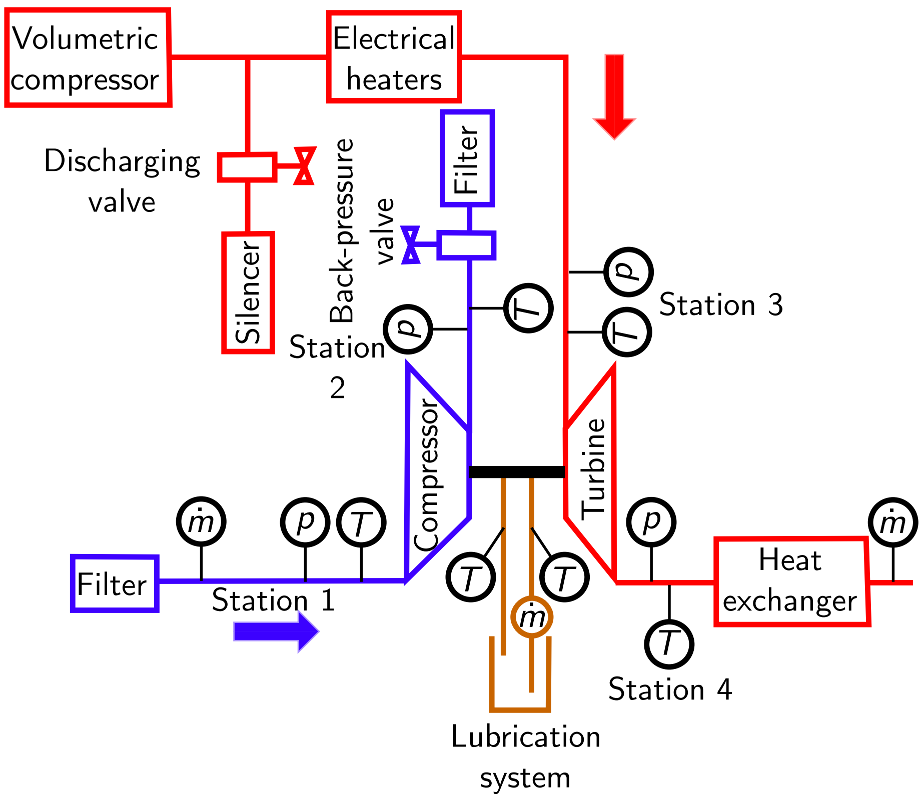

Figure 1: Schematic test bench and location of main sensors

Table 1: Characteristics of sensors employed in the test bench

Variable	Sensor	Range / Error
Gas Pressure	Piezoresistive	$[0 - 5] \pm 0.025$ bar
Air Pressure	Piezoresistive	$[0 - 2] \pm 0.025$ bar
Gas, Air and wall Temp.	K-type Therm.	$[-200 - +1200] \pm 2.2°C$
Gas and Air Flow	Hot wire	$[0 - 720] \pm 0.72$ kg/s
Oil Pressure	Piezoresistive	$[0 - 6] \pm 0.025$ bar
Oil Temperature	RTD	$[-200 - +650] \pm 0.15$ °C
Oil Flow	Coriolis	$[0 - 100]$ kg/s ± 0.1 %
Coolant pressure	Piezoresistive	$[0 - 6] \pm 0.025$ bar
Coolant Temperature	RTD	$[-200 - +650] \pm 0.15$ °C
Coolant Flow		? kg/s ± 0.1 %

allows the adjustment of these losses by a experimental [20] or a physical model [10].

2. Hot tests [9]. The main objective in this kind of tests is to obtain the convective heat fluxes in a turbocharger [21]. Besides, these tests can be divided into two groups:
   (a) External insulated tests. In these tests the whole turbocharger is externally insulated avoiding heat flows to the environment. So, only internal heat fluxes are allowed.
   (b) Exposed tests. These tests are the usually performed by manufacturers in order to obtain the turbocharger maps. The main difference with previous tests comes form the fact that heat to the environment is allowed since turbocharger is not externally insulated.

In this work, exposed tests will be performed in order to obtain external heat transfer.

2.2. Engine test rig

The test rig used to validate the proposed model in a real application, i.e. mounted on an engine, is a standard engine test rig, designed for the study of internal combustion engines up to 200 kW of power. The facility is assembled to control and evaluate the engine performance in steady and transient states. The most important devices of the engine test bench are described as follows and a scheme of the facility and its instrumentation is shown in Figure 2:

- AC- Dynamometer, variable frequency and high response.
- High frequency analogical data acquisition system.
- Last generation test room control device and data acquisition system.
- Continuous smoke measurement device.
- Control strategies design hardware.
- Airflow measurement system (Hot-wire anemometer).
- Transient fuel-flow measurement balance.
- Piezoelectric and piezoresistive cooler pressure transducer.
- Exhaust gas analyser.
- Thermocouples and Thermoresistances

The engine is installed in a bench fixed by means of metallic beams joined by screws or weldings. The structure is designed in a way that prevents the longitudinal movement of the engine and makes easier the alignment with the dynamometer.

The load rate and the engine speed are controlled by this asynchronous dynamometer (APA) and an automatic acceleration system called Throttle which are introduced into the control and data acquisition system called PUMA. The dynamometer offers the necessary resistant torque for the engine in order to test different rates of charge and dissipates the heat generated by the engine by

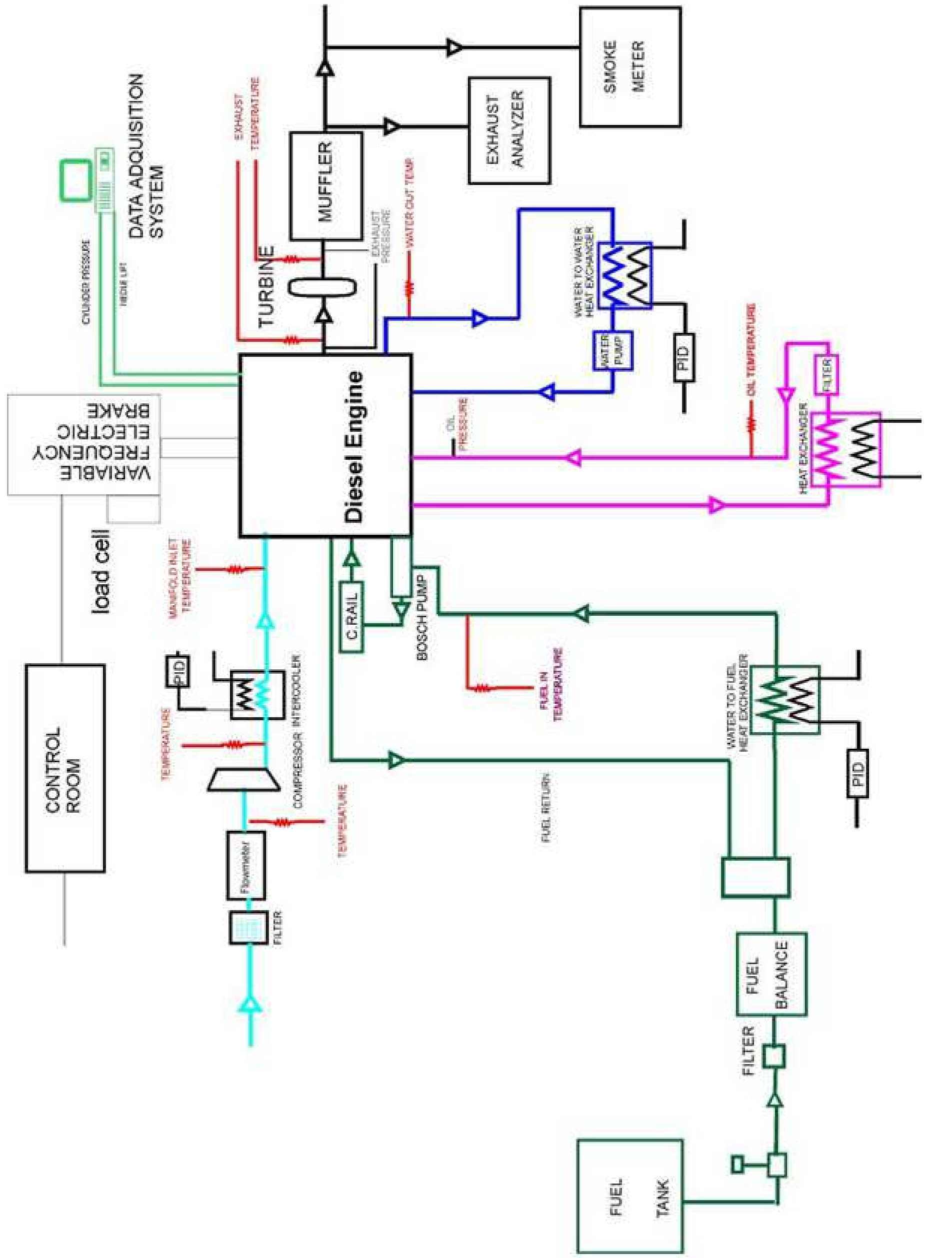

Figure 2: Layout of the engine test cell

means of water cooling systems. The thermal state of the different fluids (cooling water, admission air, fuel and oil) is controlled by means of heat exchangers, in which the mass flow of the coolant is adjusted by an electric valve controlled by a PID controller.

In an engine test bench the measurement conditions are more restrictive, although the test conditions are similar to the real operation of the turbocharger. A HDI turbocharged Diesel engine with a variable geometry turbine and an exhaust gas re-circulation valve is mounted on the facility. The main technical characteristics of this engine are presented on table 2.

Table 2: Main characteristics of the employed engine

Parameter	Value
Engine displacement [cm^3]	1997
Bore [mm]	85
Stroke [mm]	88
Number of cylinders	4 in line
Valves	4 valves per cylinder
Compression ratio	16

The facility is controlled automatically by a control system (PUMA V5) which allows the acquisition of a set of variables that characterize the behavior of the different systems of the engine. The sensors acquired by this system are of medium frequency (100 Hz). In order to acquire instantaneous (high frequency) measurements an oscillographic recorder Yokogawa DL716 digital scope (from now on YOKO) is used.

Finally, engine calculator (ECU) variables are acquired by specific control software INCA V5. Some of the measured parameters, like turbocharger pressures, are acquired by two type of sensors which are recorded by an acquisition system depending on their frequency (high or low. The torque of the engine is measured by means of a load cell coupled to the dynamometer, which speed is measured by means of an optical sensor.

The engine speed and the crankshaft rotation angle are measured by means of a Kistler 2613B optical angular encoder. The fuel flow rate is measured using a gravimetric balance (AVL-733S), allowing the measurement of both instantaneous and average fuel consumption. In the same way, as in the gas stand several instantaneous piezoresistive KISTLER pressure sensors are installed in order to measure pressure fluctuations. When no pressure fluctuations must be measured average pressure sensors are used (called FEM-P in PUMA acquisition system). For temperature measurements either Pt100 thermoresitances or type K thermocouples are used in the same way as described in section 2.1.

2.3. Turbochargers units

As it has been mentioned previously, two different turbocharger units, whose main characteristics are in Table 3 has been installed on both test rigs in order to perform the corresponding tests.

Table 3: Main characteristics of the employed turbochargers

Parameter	First turbocharger	Second turbocharger
Turbine wheel diameter [mm]	41	38
Compressor wheel diameter [mm]	49	46
VGT	yes, vanes	yes, vanes
Water cooled	yes	no

For external convection characterization of the turbocharger fifteen type K thermocouples are used, placed in five axial planes (Figure 3 shows this on turbocharger number 1). The acquisition of these sensors is performed by a datalogger Agilent 34972A unit.

3. External heat transfer model

In the case of external heat transfer, two different mechanisms are considered: radiation and convection. The proposed models for each one are explained in

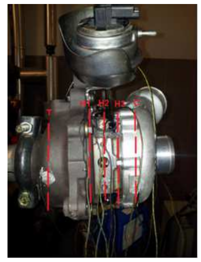

Figure 3: Photographic of wall thermocouples on Turbocharger number 1

the following sections

3.1. External radiation

The heat radiation between two gray surfaces (as the turbocharger can be considered [11]) can be calculated as [22]:

$$\dot{Q}_r = \frac{\sigma \cdot \left(T_1^4 - T_2^4\right)}{\frac{1-\varepsilon_1}{A_1 \cdot \varepsilon_1} + \frac{1}{A_1 \cdot F_{1\to 2}} + \frac{1-\varepsilon_2}{A_2 \cdot \varepsilon_2}} \tag{1}$$

where: $\dot{Q}_r$ is the net heat flux due to radiation, T is the absolute temperature of each of the surfaces, $\sigma = 5.67 \cdot 10^{-8}$ $\mathrm{W} \cdot \mathrm{m}^{-2} \cdot \mathrm{K}^{-4}$ is the Steffan-Boltzman constant, ε is the emissivity of the surface, A is the Area and F is the view factor (ratio of radiation leaving the surface and reaching another).

The exact calculation of the view factors is possible to be performed in some simple geometries (in other case, they are estimated by different mathematical algorithms such as Monte Carlo method).

In the case of a turbocharger 1D modeling programs (as GT-Power, ..) using mathematical methods is computationally unfeasible (even simplifying the complex geometry). For this reason, the turbocharger has been geometrically simplified as three cylinders (turbine, Housing and compressor) as shown in Figure 4 (where the external dimensions needs to be known)

Three different surfaces are considered in both compressor and turbine:

1. Interior surface. Disc that can interchange radiative heat transfer with the center housing.

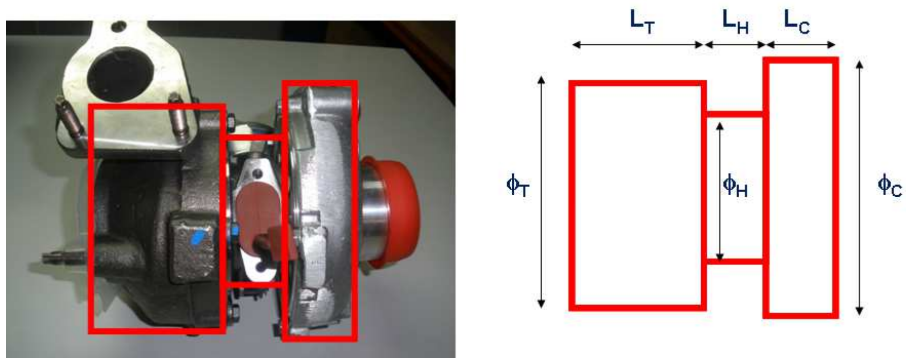

Figure 4: Simplification of turbocharger geometry

2. Exterior surface: Disc in the opposite side of central housing, it would only exchange heat to the environment (ambient, engine, . . .).
3. Lateral surface of the cylinder, it would exchange heat with the outside of the turbocharger (ambient, engine, ...).

The nodal model has three nodes in the central housing (as explained in previous works [9, 23, 24]), therefore it is necessary to have three radiant exchange surfaces, as a first approach, it was decided that this division would be:

$$\alpha_{H1} = \alpha_{H2} = \alpha_{H3} = \frac{1}{3} \tag{2}$$

According to geometrical simplification, each of the internal nodes can exchange heat by radiation with other nodes:

1. Turbine (inside surface) with H1, H2, H3, C and environment.
2. Compressor (inside surface) with H1, H2, H3, T and environment.
3. Node H1 with C, T and environment.
4. Node H2 with C, T and environment.
5. Node H3 with C, T and environment.

3.1.1. Calculation of view factors for each surface

In the literature, the following analytic expressions of the view factors can be found:

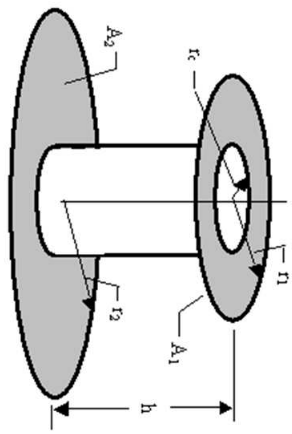

Figure 5: Two concentric discs separated by a concentric cylinder

1. Between two concentric discs separated by a concentric cylinder (Figure 5 and equation 3) [25]:

$$F_{1\to 2} = \frac{1}{\pi \cdot A}\left[\begin{array}{c} \frac{A}{2}\cos^{-1}\frac{R_c}{R_2} + \frac{B}{2}\cos^{-1}\frac{R_c}{R_1} + 2R_c\left(\tan^{-1}Y - \tan^{-1}A^{1/2} - \tan^{-1}B^{1/2}\right) \\ -\left[\left(1+C^2\right)\left(1+D^2\right)\right]^{1/2}\tan^{-1}\left[\frac{\left(1+C^2\right)\left(Y^2-D^2\right)}{\left(1+D^2\right)\left(C^2-Y^2\right)}\right]^{1/2} \\ +\left\{\left[1+\left(R_1+R_c\right)^2\right]\left[1+\left(R_1-R_c\right)^2\right]\right\}^{1/2}\tan^{-1}\left\{\frac{\left[1+\left(R_1+R_c\right)^2\right]\left(R_1-R_c\right)}{\left[1+\left(R_1-R_c\right)^2\right]\left(R_1+R_c\right)}\right\}^{1/2} \\ +\left\{\left[1+\left(R_2+R_c\right)^2\right]\left[1+\left(R_2-R_c\right)^2\right]\right\}^{1/2}\tan^{-1}\left\{\frac{\left[1+\left(R_2+R_c\right)^2\right]\left(R_2-R_c\right)}{\left[1+\left(R_2-R_c\right)^2\right]\left(R_2+R_c\right)}\right\}^{1/2} \end{array}\right] \tag{3}$$

where:

$$\begin{array}{l} R_1 = \frac{r_1}{h} \quad R_2 = \frac{r_2}{h} \quad R_c = \frac{r_c}{h} \quad A = R_1^2 - R_c^2 \\ B = R_2^2 - R_c^2 \quad C = R_2 + R_1 \quad D = R_2 - R_1 \quad Y = A^{1/2} + B^{1/2} \end{array} \tag{4}$$

2. Between a ring and a cylinder lateral surface (Figure 6 and equation 5)

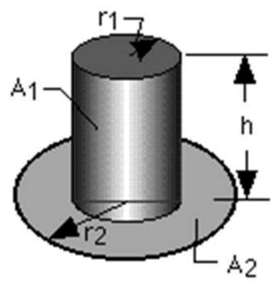

Figure 6: A ring and a cylinder lateral surface

[26]:

$$F_{1\to 2} = \frac{B}{8RH} + \frac{1}{2\pi}\left\{\cos^{-1}\left(\frac{A}{B}\right) - \frac{1}{2H}\left[\frac{(A+2)^2}{R^2} - 4\right]^{1/2}\cos^{-1}\left(\frac{AR}{B}\right) - \frac{A}{2RH}\sin^{-1} R\right\} \tag{5}$$

where:

$$R = \frac{r_1}{r_2} \quad H = \frac{h}{r_2} \quad A = H^2 + R^2 - 1 \quad B = H^2 - R^2 + 1 \tag{6}$$

The different view factors of the simplified geometry (Figure 4) can be calculated using the previous analytic expressions and the properties of the view factors [22]: reciprocity (equation 7), summation (equation 8) and subdivision (equation 9),

$$F_{1\to 2} A_1 = F_{2\to 1} A_2 \tag{7}$$

$$\sum_j F_{i\to j} = 1 \tag{8}$$

$$F_{j\to i} = \frac{\sum_{k=1}^{n} A_k F_{k\to i}}{\sum_{k=1}^{n} A_k} \tag{9}$$

So the view factors in the internal part of the turbocharger can be calculated following this methodology:

View Factors in turbine side:

1. F_{T-C}: The view factor between turbine and compressor can be calculated:

   (a) If turbine diameter, ϕ_T, is smaller than compressor external diameter, ϕ_C, using directly the analytic expression of view factor between two concentric discs separated by a concentric cylinder, using Equations 3 and 4.

   (b) Otherwise, the same expression (Equations 3 and 4) can be used to calculate the view factor between compressor and turbine, F_{C-T}, and then applying the reciprocity property of view factors (Equation 7), one can lead to:

$$F_{T-C} = \frac{F_{C-T} \cdot A_C}{A_T} = F_{C-T} \frac{\phi_C^2 - \phi_H^2}{\phi_T^2 - \phi_H^2} \tag{10}$$

2. F_{T-H1}: The view factor between turbine and H1 nodes can be calculated in two steps methodlogy:

   (a) Using the analytic expression of view factor between a ring and a cylinder lateral surface (ie: obtaining F_{H1-T}) using Equations 5 and 6

   (b) applying the reciprocity property (Equation 7):

$$F_{T-H1} = \frac{F_{H1-T} \cdot A_{H1}}{A_T} = F_{H1-T} \frac{4 \cdot \alpha_{H1} \cdot L_H \cdot \phi_H}{\phi_T^2 - \phi_H^2} \tag{11}$$

3. F_{T-H2}: in this case the methodology is:

   (a) Applying the subdivision property (Equation 9) by defining a surface composed by H1 and H2 external surfaces:

$$F_{T-H2} = F_{T-H1+H2} - F_{T-H1} \tag{12}$$

   (b) Now, the view factor $F_{T-H1+H2}$ can be calculated as F_{T-H1} with different geometrical length, i.e.:

$$F_{T-H1+H2} = F_{H1+H2-T} \frac{A_{H1+H2}}{A_T} = F_{H1+H2-T} \frac{4 \cdot (\alpha_{H1} + \alpha_{H2}) \cdot L_H \cdot \phi_H}{\phi_T^2 - \phi_H^2} \tag{13}$$

where $F_{H1+H2-T}$ is calculated as the view factor between a ring and a cylinder lateral surface (Equations 5 and 6)

4. F_{T-H3}, the methodology is similar to the one explained for F_{T-H2}:
   (a) Apply the subdivision property by defining a surface composed by H1, H2 and H3 external surfaces, so:

$$F_{T-H3} = F_{T-H1+H2+H3} - F_{T-H1+H2} \tag{14}$$

being:

- $F_{T-H1+H2+H3} = F_{H1+H2+H3-T} \frac{A_{H1+H2+H3}}{A_T}$
- $F_{H1+H2+H3-T}$ is calculated as the view factor between a ring and a cylinder lateral surface (Equations 5 and 6)
- the ratio between the areas is: $\frac{A_{H1+H2+H3}}{A_T} = \frac{4 \cdot L_H \cdot \phi_H}{\phi_T^2 - \phi_H^2}$

5. Finally, the view factor between turbine and the ambient is calculated using the summation property (Equation 8) as:

$$F_{T-amb} = 1 - (F_{T-H1} + F_{T-H2} + F_{T-H3} + F_{T-C}) \tag{15}$$

View Factors in Compressor side:

1. F_{C-T}: in the case the compressor external diameter, ϕ_C would be smaller that the turbine external diameter, ϕ_C, this view factor has been already calculated (see 1 in the view factor in turbine side (section 3.1.1), otherwise the reciprocity property (Equation 7) is applied:

$$F_{C-T} = \frac{F_{T-C} \cdot A_T}{A_C} = F_{T-C} \frac{\phi_T^2 - \phi_H^2}{\phi_C^2 - \phi_H^2} \tag{16}$$

where F_{T-C} is already known (1 of section 3.1.1 the turbine side calculations)

2. F_{C-H3}. The view factor between compressor and H3 nodes can be calculated in two steps:
   (a) Using the analytic expression of view factor between a ring and a cylinder lateral surface (i.e: obtaining F_{H3-C}) using Equations 5 and 6

(b) Applying the reciprocity property (Equation 7):

$$F_{C-H3} = \frac{F_{H3-C} \cdot A_{H3}}{A_C} = F_{H3-C} \frac{4 \cdot \alpha_{H3} \cdot L_H \cdot \phi_H}{\phi_C^2 - \phi_H^2} \tag{17}$$

3. F_{C-H2}: in this case the methodology is:

   (a) Applying the subdivision property (Equation 9) by defining a surface composed by H2 and H3 external surfaces:

$$F_{C-H2} = F_{C-H2+H3} - F_{C-H3} \tag{18}$$

   (b) Now, the view factor $F_{C-H2+H3}$ can be calculated as F_{C-H3} with different geometrical length, i.e.:

$$F_{C-H2+H3} = F_{H2+H3-C} \frac{A_{H2+H3}}{A_C} = F_{H2+H3-C} \frac{4 \cdot (\alpha_{H2} + \alpha_{H3}) \cdot L_H \cdot \phi_H}{\phi_C^2 - \phi_H^2} \tag{19}$$

   where $F_{H2+H3-C}$ is calculated as the view factor between a ring and a cylinder lateral surface (Equations 5 and 6)

4. F_{C-H1}, the methodology is similar to the one explained for F_{T-H3} (see point 4 in section 3.1.1)

   (a) Apply the subdivision property by defining a surface composed by H1, H2 and H3 external surfaces, so:

$$F_{C-H1} = F_{C-H1+H2+H3} - F_{C-H2+H3} \tag{20}$$

   being:

   - $F_{C-H1+H2+H3} = F_{H1+H2+H3-C} \frac{A_{H1+H2+H3}}{A_C}$
   - $F_{H1+H2+H3-C}$ is calculated as the view factor between a ring and a cylinder lateral surface (Equations 5 and 6)
   - the ratio between the areas is: $\frac{A_{H1+H2+H3}}{A_C} = \frac{4 \cdot L_H \cdot \phi_H}{\phi_C^2 - \phi_H^2}$

5. Finally, the view factor between compressor and the ambient is calculated using the summation property (Equation 8) as:

$$F_{C-amb} = 1 - (F_{C-H1} + F_{C-H2} + F_{C-H3} + F_{C-T}) \tag{21}$$

View Factors in Central housing:

1. Two of the needed view factors are already calculated:
   - F_{H1-T} (see 2 of section 3.1.1)
   - F_{H3-C} (see 2 of section 3.1.1).
2. The view factors: F_{H2-T}, F_{H3-T}, F_{H1-C} and F_{H2-C}; can be calculated using the reciprocity property (Equation 7) and already calculated view factors: F_{T-H2}, F_{T-H3}, F_{C-H1} and F_{C-H2} (points 3 and 4 in section 3.1.1 and points 4 and 3 in section 3.1.1 respectively), leading to:

$$F_{H2-T} = F_{T-H2}\frac{A_T}{A_{H2}} = F_{T-H2}\frac{\phi_T^2 - \phi_H^2}{4 \cdot \alpha_{H2} \cdot L_H \cdot \phi_H} \tag{22}$$

$$F_{H3-T} = F_{T-H3}\frac{A_T}{A_{H3}} = F_{T-H3}\frac{\phi_T^2 - \phi_H^2}{4 \cdot \alpha_{H3} \cdot L_H \cdot \phi_H} \tag{23}$$

$$F_{H1-C} = F_{C-H1}\frac{A_C}{A_{H1}} = F_{C-H1}\frac{\phi_C^2 - \phi_H^2}{4 \cdot \alpha_{H1} \cdot L_H \cdot \phi_H} \tag{24}$$

$$F_{H2-C} = F_{C-H2}\frac{A_C}{A_{H2}} = F_{C-H2}\frac{\phi_C^2 - \phi_H^2}{4 \cdot \alpha_{H2} \cdot L_H \cdot \phi_H} \tag{25}$$

3. Finally, the view factor between housing nodes and the ambient are calculated using the summation property (Equation 8) as:

$$F_{H1-amb} = 1 - (F_{H1-C} + F_{H1-T}) \tag{26}$$

$$F_{H2-amb} = 1 - (F_{H2-C} + F_{H2-T}) \tag{27}$$

$$F_{H3-amb} = 1 - (F_{H3-C} + F_{H3-T}) \tag{28}$$

3.1.2. Radiation to the ambient

For radiation to ambient Equation 1 is simplified to:

$$\dot{Q}_r = \frac{\varepsilon_1 \cdot F_{1\to2}}{\varepsilon_1 \cdot (1 - F_{1\to2}) + F_{1\to2}} A_1 \cdot \sigma \cdot \left(T_1^4 - T_{amb}^4\right) \tag{29}$$

Then, in the case of the turbine and the compressor, the surfaces that do not see the internal part of the turbocompressor (i.e,: lateral and external casings) must be also taken into account. Therefore the whole radiative heat transfer for these nodes can be calculated as:

$$\begin{aligned}\dot{Q}_{Ttotal-amb} &= \dot{Q}_{T-amb} + \dot{Q}_{Tlat-amb} + \dot{Q}_{Text-amb} \\ &= \left(\frac{\frac{\pi}{4}\phi_T^2 \cdot F_{T\to amb}}{\varepsilon_T \cdot (1 - F_{T\to amb}) + F_{T\to amb}} + \pi \cdot \phi_T \cdot L_T + \frac{\pi}{4}\phi_T^2 \right) \cdot \varepsilon_T \cdot \sigma \cdot \left(T_T^4 - T_{amb}^4\right) \\ &= \left(\phi_T \cdot \left[1 + \frac{F_{T\to amb}}{\varepsilon_T \cdot (1 - F_{T\to amb}) + F_{T\to amb}} \right] + 4 \cdot L_T \right) \cdot \frac{\pi}{4} \cdot \phi_T \cdot \varepsilon_T \cdot \sigma \cdot \left(T_T^4 - T_{amb}^4\right)\end{aligned} \tag{30}$$

$$\begin{gathered}\dot{Q}_{Ctotal-amb} = \dot{Q}_{C-amb} + \dot{Q}_{Clat-amb} + \dot{Q}_{Cext-amb} = \\ = \left(\frac{\frac{\pi}{4}\phi_C^2 \cdot F_{C\to amb}}{\varepsilon_C \cdot (1 - F_{C\to amb}) + F_{C\to amb}} + \pi \cdot \phi_C \cdot L_C + \frac{\pi}{4}\phi_C^2 \right) \cdot \varepsilon_C \cdot \sigma \cdot \left(T_C^4 - T_{amb}^4\right) = \\ = \left(\phi_C \cdot \left[1 + \frac{F_{C\to amb}}{\varepsilon_C \cdot (1 - F_{C\to amb}) + F_{C\to amb}} \right] + 4 \cdot L_C \right) \cdot \frac{\pi}{4} \cdot \phi_C \cdot \varepsilon_C \cdot \sigma \cdot \left(T_C^4 - T_{amb}^4\right)\end{gathered} \tag{31}$$

In the case that one of the surfaces had a radiation shield (typical in turbine side) a procedure has been developed in order to avoid the inclusion of new nodes. The methodology consists on changing the view factor between the shielded surface and the others, which has been possible assuming that the external surface of the shielded surface is the same as the non-shielded. Comparing the heat fluxes between two gray surfaces with (Equation 32) and without shield (Equation 1) and after some calculations one can led to equation 33:

$$\dot{Q}_r = \frac{\sigma \cdot \left(T_1^4 - T_2^4\right)}{\frac{1-\varepsilon_1}{A_1 \cdot \varepsilon_1} + \frac{2}{A_1 \cdot F_{1\to 2}} + 2 \cdot \frac{1-\varepsilon_s}{A_1 \cdot \varepsilon_s} + \frac{1-\varepsilon_2}{A_2 \cdot \varepsilon_2}} \tag{32}$$

$$F_{1s\to 2} = \frac{F_{1\to 2}}{2} \left(\frac{\varepsilon_s}{F_{1\to 2} + \varepsilon_s \left(1 - F_{1\to 2}\right)} \right) \tag{33}$$

3.2. External Convection.

In the case of external convection, three cases are considered: free, forced and mixed convection:

3.2.1. *Free convection*

The geometric simplification is the same that in external radiation (see Figure 4). The calculation of the convective conductances between the ambient air and each of the five metal nodes is calculated as:

$$K_{CN} = h_{CN} \cdot A = h_{CN} \cdot \pi \cdot L \cdot \phi \tag{34}$$

The coefficient of heat transfer by free convection, h_{CN} , is calculated from the correlation of Churchill and Chu [27]:

$$\overline{\mathrm{Nu}_{D,CN}} = \left\{ 0.6 + \frac{0.387 \cdot \mathrm{Ra}_D^{1/6}}{\left[1 + (0.559/\mathrm{Pr})^{9/16}\right]^{8/27}} \right\}^2 \tag{35}$$

where: $\mathrm{Ra}_D = \mathrm{Gr} \cdot \mathrm{Pr}$ is the Rayleigh number, $\mathrm{Gr} = \frac{g \cdot \beta \cdot (T_w - T_{amb}) \cdot \phi^3}{\upsilon^2}$ is the Grasshof number; $\beta = \frac{1}{(T_w + T_{amb})/2}$ and υ is the kinematic viscosity.

All the properties in Equation 35 are calculated at mean temperature between wall, T_w, and fluid, T_{amb}

3.2.2. *Forced convection*

In the case of forced convection, the used correlation [28] correspond to the perpendicular flow through a horizontal cylinder:

$$\overline{\mathrm{Nu}_{D,CF}} = 0.3 + \frac{0.62 \cdot \mathrm{Re}_D^{1/2} \cdot \mathrm{Pr}^{1/3}}{\left[1 + (0.4/\mathrm{Pr})^{2/3}\right]^{1/4}} \left[1 + \left(\frac{\mathrm{Re}_D}{282000}\right)^{5/8}\right]^{4/5} \tag{36}$$

All the properties in Equation 36 are calculated at mean temperature between wall, T_w, and fluid, T_{amb} and it is valid for $\mathrm{Re}_D \cdot \mathrm{Pr} \geq 0.2$

3.2.3. *Mixed Convection*

In the case that there is no predominant kind of convection (forced or free) a mixed of both is used. Therefore Equation 37 is used:

$$0.1 \leq \frac{\mathrm{Gr}_D}{\mathrm{Re}_D^2} \leq 10 \rightarrow \overline{\mathrm{Nu}_D}^3 = \overline{\mathrm{Nu}_{D,CN}}^3 + \overline{\mathrm{Nu}_{D,CF}}^3 \tag{37}$$

4. Validation of the model

In order to validate the presented turbocharger external heat transfer model, exposed measurements in the gas stand test rig, explained on section 2.1, were performed and used. Figure 7 show the measured points in both compressor and turbine maps. Only one VGT position has been measured for turbocharger 1 (corresponding to a 40 % opening) and 2 positions for turbocharger 2 (30 and 15 % respectively).

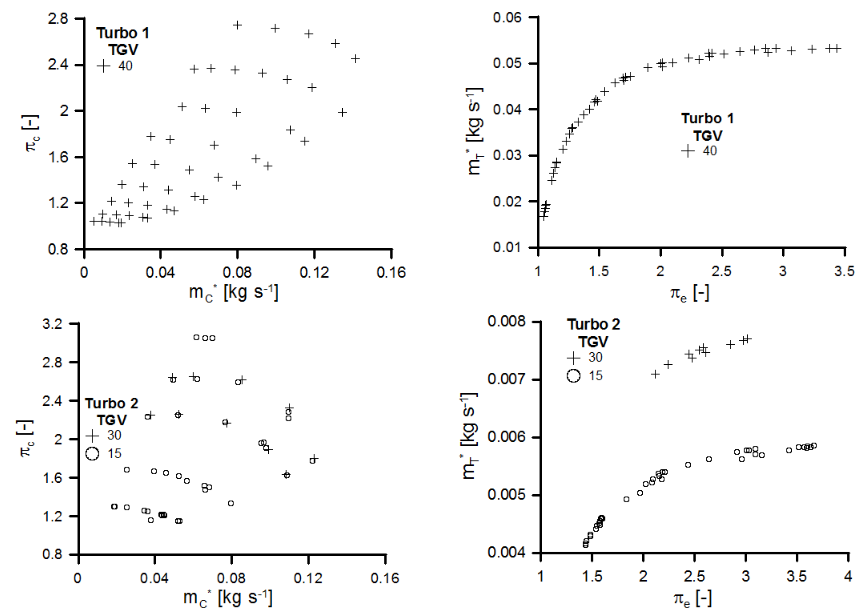

Figure 7: Measured points in exposed tests

4.1. Experimental external heat transfer

In exposed tests, turbocharger can exchange energy with environment. In order to obtain external heat transfer an energy balance has been performed [12], i.e. the measured energy unbalance is assumed to be equal to external heat transfer. The advantage of this approach is the simplicity (equation 38) but its main disadvantage is that only global behavior can be determined (that is, the contribution of the different nodes to external losses can not be determined directly neither the possible interactions among them). Nevertheless, the most important contribution to external heat transfer to the environment will be the turbine, due to its higher temperature (radiative contribution) and big contact area:

$$\begin{aligned}\dot{Q}_{ext} \approx \dot{Q}_{unb} = \sum_i \dot{m}_i \cdot \Delta h_i = \\ = \dot{m}_{gas} \cdot \Delta h_{gas} + \dot{m}_{air} \cdot \Delta h_{air} + \dot{m}_{oil} \cdot \Delta h_{oil} + \dot{m}_{cool} \cdot \Delta h_{cool} = \\ = \dot{m}_T \cdot \overline{c_{p,T}} \cdot (T_{IT} - T_{OT}) + \dot{m}_C \cdot \overline{c_{p,C}} \cdot (T_{IC} - T_{OC}) + \\ \dot{m}_{oil} \cdot \overline{c_{p,oil}} \cdot (T_{IO} - T_{OO}) + \dot{m}_{cool} \cdot \overline{c_{p,cool}} \cdot (T_{IC} - T_{OC})\end{aligned} \tag{38}$$

4.2. Adjustment external heat transfer models.

Figure 8 shows the comparison between unbalance results and the estimated by the external heat transfer model (see section 3, where the main parameters are shown in Table 4 and air velocity in the benches has been imposed to 1 ms^{-1} after some measurements performed.

Table 4: Values used in the model

Parameter	**Zone** T	H	C	**Source**
ϵ	0.93	0.93	0.64	[11] and thermographic measurements
ϕ [mm]	122	70	123	Measured
L [mm]	70	31	32	Measured

As Figure 8 shows, the agreement is reasonable, but it seems the proposed external heat transfer model (it must be pointed out that the model means a high geometric simplification and no adjustment constant has been used) underestimate the experimental values. This deviation is small compared with turbine enthalpy drop as can be shown in Figure 9 where the dimensionless difference between measured external heat transfer and the one obtained directly with external heat transfer model are presented. As Figure 9 shows, the main differences come at low turbine enthalpy drops, being in this case below than 10 % while it is lower than a 3 % at high turbine powers, i.e. $N_T > 3kW$.

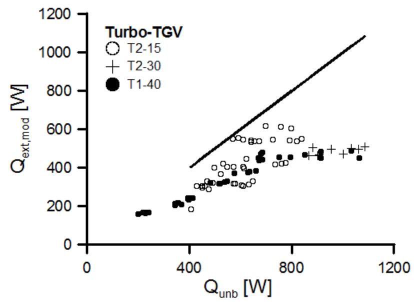

Figure 8: Comparison between measured external heat transfers and model prediction

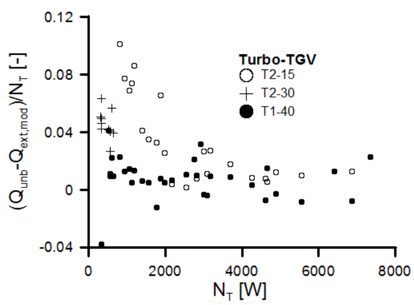

Figure 9: Difference, in dimensionless form, between measured external heat transfer and model results

In order to adjust the proposed external model and knowing that the most significant geometrical parameter will be the Turbine external diameter, an adjustment parameter of this diameter has been included:

$$\phi_T = \psi_T \cdot \mathrm{D_t} \tag{39}$$

Results of the adjustment are shown in Figure 10 where, for both turbochargers, $\psi_T = 1.25$, which means an increment of effective surface respect to the proposed cylinder used for turbine simplification. It is justified watching at Figure 4, where turbine flanges were not included inside the proposed simplification of turbine geometry.

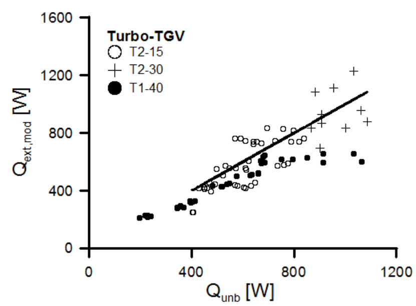

Figure 10: Comparison between external heat transfers: adjusted external model and unbalance method

4.3. Validation of external heat transfer models.

In order to validate the proposed model, both turbochargers were installed on an engine (section 2.2): the external heat transfer has been obtained as explained in section 4.1. Figure 11 shows the same data of Figure 10 but including the data from engine test measurements, where a good agreement is observed.

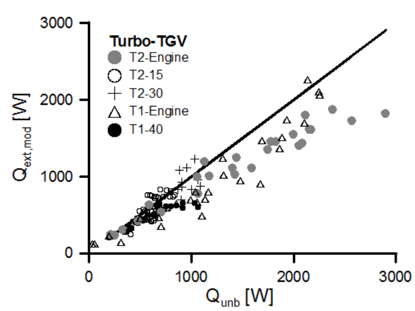

Figure 11: Comparison between external heat transfers: adjusted external model and unbalance method in engine

Maximum turbine inlet temperature was about 450 °C in gas stand tests used for model elaboration, but around 900 °C in engine tests used for proposed model validation.

5. Model application

Once the external heat transfer model has been validated, it has been used in order to estimate the different heat flows among turbochargers nodes. Figure 12 shows the external heat (absorbed or lost) by each of the five nodes compared to the total enthalpy drop in the turbine, the following conclusions can be extracted:

- The main important external heat losses comes from turbine node (they can reach up to a half of the turbine enthalpy drop. This fact can be explained by two main reasons: on one hand the high temperature of the turbine external surface and, on the other, the high exposed area.
- In compressor side, in most of the cases, heat is absorbed by the compressor case (negative values), indicating that compressor case is receiving a higher heat from turbine side by radiation than the heat lost to the ambient (both convective and radiative).
- External heat fluxes at housing nodes is almost negligible compared to the turbine enthalpy drop. They are about two order of magnitude lower than heat losses from turbine node.

Due to the previous results a deeper study on heat transfer in turbine and compressor side has been performed.

5.1. Turbine side

Figure 13 shows the external heat flows obtained in the turbine side for both turbocompressors, where it is observed that the radiation heat flux is almost equal to the total heat lost by the turbine (left top of Figure 13), while convective heat losses (right top of Figure 13) are negligible in comparison. The different radiation losses in turbine are shown in the left bottom of Figure 13 where the most important contribution is due to ambient losses, but right bottom of Figure 13 shows a zoom of left bottom of Figure 13 where it is shown that the radiation to compressor is quite more important that radiation to the other nodes.

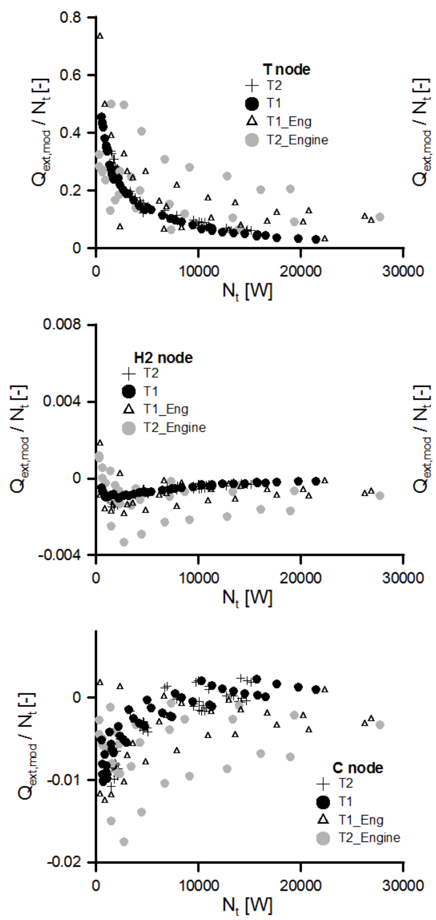

Figure 12: Importance of modeled external heat fluxes compared to turbine enthalpy drop

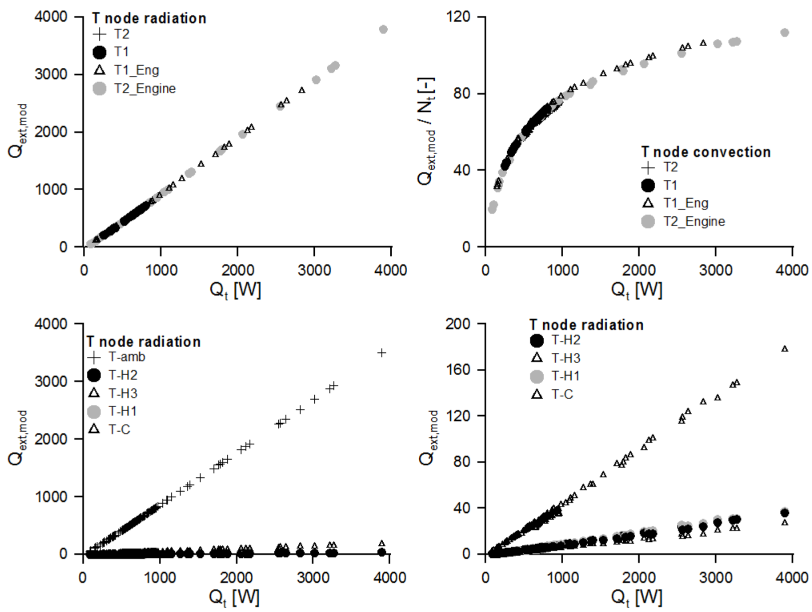

Figure 13: Analysis of modeled external heat transfer in turbine side

5.2. *Compressor side*

In compressor side, external heat fluxes can be reversed, i.e. compressor can absorb some heat from the enviroment (mostly from the turbine case). Top left of Figure 14 shows that, as in the case of the turbine, the whole external heat to/from compressor is almost equal to the radiative part, while top right of Figure 14 indicates that convective heat losses has no any clear relationship with total external heat of compressor. Finally, bottom of Figure 14 indicates that the most important radiative heat flux comes from turbine side, but due to the smaller quantities the other fluxes cannot be neglected.

6. Conclusions

Traditionally, heat losses in small turbochargers has been neglected and the behavior of the machine has been predicted by direct use of manufacturer maps. But at low loads, this energy transfer can reach values even higher than mechanical power.

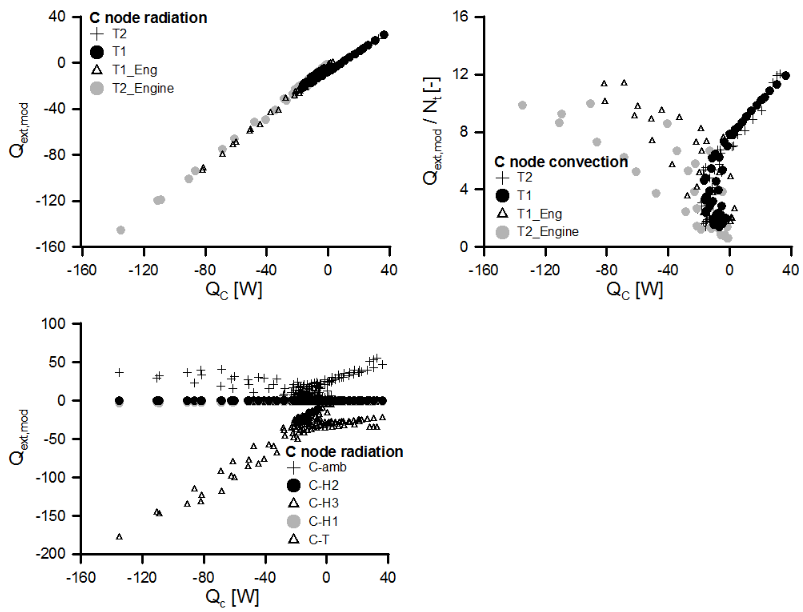

Figure 14: Analysis of modeled external heat transfer in compressor side

This work presents a external heat transfer model that takes into account radiation and convective phenomena and all the possible paths of heat from turbocharger external surfaces. The model uses a simplified geometry, based on cylinders, of the whole turbocharger.

The proposed model has been adjusted against experimental measurements on two different turbocharges in a turbocharger test bench. The validation of the model has been performed by comparing the model predictions with experiments performed on an engine test bench.

The adjusted and validated model has been used to perform an analysis of the different heat flows, showing that:

- The most important external heat fluxes comes from turbine external surface, due to its higher temperature and its big areas. They can lead to be up to a half of turbine enthalpy drop.

- External heat fluxes at the central housing are negligible compared to the turbine enthalpy drop

- In compressor side, external heat flow can be reversed, i.e. it can be lost or absorbed depending on the running conditions. In this side, the most important seems to be the heat radiated by the turbines side but the other paths can not be neglected.

Acknowledgments

This work has been financial supported by Jaguar Land Rover Ltd.

References

[1] S. Jaichandar, K. Annamalai, Combined impact of injection pressure and combustion chamber geometry on the performance of a biodiesel fueled diesel engine, Energy 55 (2013) 330 – 339.

[2] A. J. Torregrosa, A. Broatch, R. Novella, L. F. Mónico, Suitability analysis of advanced diesel combustion concepts for emissions and noise control, Energy 36 (2011) 825 – 838.

[3] I. Al-Hinti, M. Samhouri, A. Al-Ghandoor, A. Sakhrieh, The effect of boost pressure on the performance characteristics of a diesel engine: A neuro-fuzzy approach., Applied Energy 86 (2009) 113–121.

[4] J. R. Serrano, F. J. Arnau, V. Dolz, A. Tiseira, M. Lejeune, N. Auffret, Analysis of the capabilities of a two-stage turbocharging system to fulfil the US2007 anti-pollution directive for heavy duty diesel engines, International Journal of Automotive Technology 9 (2008) 277–288.

[5] V. Bermúdez, J. M. Luján, B. Plá, W. G. Linares, Effects of low pressure exhaust gas recirculation on regulated and unregulated gaseous emissions during nedc in a light-duty diesel engine, Energy 36 (2011) 5655 – 5665.

[6] M. Jia, Y. Li, M. Xie, T. Wang, Numerical evaluation of the potential of late intake valve closing strategy for diesel {PCCI} (premixed charge

compression ignition) engine in a wide speed and load range, Energy 51 (2013) 203 – 215.

[7] B. Prasad, C. Sharma, T. Anand, R. Ravikrishna, High swirl-inducing piston bowls in small diesel engines for emission reduction, Applied Energy 88 (2011) 2355 – 2367.

[8] B. Kegl, Influence of biodiesel on engine combustion and emission characteristics, Applied Energy 88 (2011) 1803–1812.

[9] J. R. Serrano, P. Olmeda, F. J. Arnau, M. A. Reyes-Belmonte, A. Lefebvre, Importance of heat transfer phenomena in small turbochargers for passenger car applications, SAE Int. J. Engines 6 (2013) 2013–01–0576.

[10] J. R. Serrano, P. Olmeda, A. Tiseira, L. M. García-Cuevas, A. Lefebvre, Theoretical and experimental study of mechanical losses in automotive turbochargers, Energy 55 (2013) 888–898.

[11] D. Bohn, N. Moritz, M. Wolff, Conjugate Flow and Heat Transfer Investigation of a Turbo Charger: Part II — Experimental Results, in: Proceedings of ASME Turbo Expo, volume 3, ASME, 2003, pp. 723–729.

[12] N. Baines, K. D. Wygant, A. Dris, The analysis of heat transfer in automotive turbochargers, Journal of Engineering for Gas Turbineas and Power - Transactions of the ASME 132 (2010) 42301.

[13] A. Romagnoli, R. Martínez-Botas, Heat transfer on a turbocharger under constant load points, in: Proceedings of ASME Turbo Expo, volume 5, pp. 163–174.

[14] A. Romagnoli, R. Martínez-Botas, Heat transfer analysis in a turbocharger turbine: An experimental and computational evaluation, Applied Thermal Engineering 38 (2012) 58–77.

[15] H. Aghaali, H.-E. Ångstrom, Turbocharged SI-engine simulation with cold and hot-measured turbocharger performance maps, in: Proceeding of ASME Turbo Expo, pp. GT2012–68758.

[16] Society of Automotive Engineers, Supercharger testing standard, SAE SAE J1723 (1995).

[17] Society of Automotive Engineers Inc, Turbocharger gas stand test code, SAE SAE J1826 (1995).

[18] S. Shaaban, Experimental Investigation and Extended Simulation of Turbocharger Non-Adiabatic Performance, Ph.D. thesis, Universitat Hannover, Fachbereich Maschinenbau, 2004.

[19] J. R. Serrano, P. Olmeda, A. Tiseira, L. M. García-Cuevas, A. Lefebvre, Importance of mechanical losses modelling in the performance prediction of radial turbochargers under pulsating flow conditions, SAE Int. J. Engines 6 (2013) 2013–01–0576.

[20] F. Payri, J. R. Serrano, P. Olmeda, A. Páez, F. Vidal, Experimental Methodology to Characterize Mechanical Losses in Small Turbochargers, in: Proceedings of the ASME Turbo Expo 2010, volume 5, pp. 413–424.

[21] J. R. Serrano, P. Olmeda, F. J. Arnau, M. A. Reyes-Belmonte, A. Lefebvre, H. Tartoussi, A study on the internal convection in small turbochargers, Submitted to Energy (2013).

[22] F. P. Incropera, D. P. Dewitt, T. L. Bergman, A. S. Lavine, Fundamentals of Heat and Mass Transfer, John Wiley & Sons, Inc., 111 River Street, Hoboken, NJ 0703-5774, 6th edition, 2007.

[23] P. Olmeda, V. Dolz, F. J. Arnau, M. A. Reyes-Belmonte, Determination of heat flows inside turbochargers by means of a one dimensional lumped model, Mathematical and Computer Modelling 57 (2013) 1847 – 1852.

[24] J. R. Serrano, P. Olmeda, A. Páez, F. Vidal, An experimental procedure to determine heat transfer properties of turbochargers, Measurement Science and Technology 21 (2010) 035109 (14pp).

[25] D. Bornside, R. Brown, View factor between differing-diameter, coaxial disks blocked by a coaxial cylinder, J. Thermophys. Heat Transfer 4 (1990) 414–416.

[26] E. Sparrow, G. Miller, V. Jonsson, Radiative effectiveness of annular- finned space radiators, including mutual irradiation between radiator elements, J. Aerospace Sci. 29 (1962) 1291–1299.

[27] S. W. Churchill, H. H. Chu, Correlating equations for laminar and turbulent free convection from a horizontal cylinder, International Journal of Heat and Mass Transfer 18 (1975) 1049 – 1053.

[28] S. W. Churchill, M. Bernstein, A correlating equation for forced convection from gases and liquids to a circular cylinder in crossflow, Journal of Heat Transfer 99 (1977) 300–306.